Appl. Phys. A 76, 621–623 (2003)
DOI: 10.1007/s00339-002-2029-9

Applied Physics A
Materials Science & Processing

F.C. FONSECA[1]
G.F. GOYA[1]
R.F. JARDIM[1,✉]
N.L.V. CARREÑO[2]
E. LONGO[2]
E.R. LEITE[2]
R. MUCCILLO[3]

Magnetic properties of Ni:SiO_2 nanocomposites synthesized by a modified sol–gel method

[1] Instituto de Física, Universidade de São Paulo, CP 66318, 05315-970, São Paulo, SP, Brazil
[2] Centro Multidisciplinar de Desenvolvimento de Materiais Cerâmicos CMDMC, Departamento de Química, Universidade Federal de São Carlos, CP 676, 13560-905, São Carlos, SP, Brazil
[3] Centro Multidisciplinar de Desenvolvimento de Materiais Cerâmicos CMDMC, CCTM-Instituto de Pesquisas Energéticas e Nucleares, CP 11049, 05422-970, São Paulo, SP, Brazil

Received: 7 October 2002/Accepted: 9 October 2002
Published online: 8 January 2003 •

ABSTRACT Ni nanoparticles embedded in an amorphous SiO_2 matrix were produced by a modified sol–gel method. This method resulted in nanocomposites with a controlled size distribution and good dispersion of the metallic particles. The particle-size distributions were found to have an average radius of ~ 3 nm, as inferred from transmission electron microscopy, X-ray-diffraction analysis, and magnetic measurements. Magnetic characterizations revealed that samples exhibit superparamagnetic behavior above the blocking temperature T_B, $20\,K \leq T_B \leq 40\,K$, and absence of a shift along the field axis on hysteresis loops measured at $T \leq T_B$, indicating that the metallic nanoparticles are also free from an oxide layer.

PACS 75.50.Tt; 75.75.+a; 81.16.Be; 75.20.-g; 75.20.En

Nanostructured magnetic materials have attracted great interest due to the novel properties that originate from finite-size effects, size distributions (SDs), and interparticle interactions [1, 2]. Recent effort has been focused on the development of nanostructured magnetic materials due to their potential applications [1]. Particularly, nanoparticles (NPs) of ferromagnetic (FM) metals such as Co [3], Fe [4], and Ni [5, 6] have been prepared by different methods in which the control of the processing parameters plays a major role. Examples of reported synthetic techniques for the fabrication of these NPs include the decomposition of organometallic precursors [7], the reduction of metal salts [8], and ionic implantation [9]. In all cases, parameters of the preparation method must be carefully controlled to obtain a desired particle SD without agglomeration. In addition, as a result of the processing method, an oxide surface layer can be formed, leading to a shell–core morphology where an antiferromagnetic (AFM) oxide layer surrounds the FM metallic NP. Such a morphology influences the magnetic properties due to the exchange interaction between the FM and AFM phases.

Besides the processing technique used, an approach to assemble and maintain a nanostructured material is to host the metallic NP in an inorganic and non-magnetic matrix. The development of nanocomposites, in which metallic particles are embedded in a matrix, can provide an effective way of tailoring a uniform SD and of controlling the dispersion of ultra-fine particles [10].

In this letter, we describe a modified sol–gel method for preparing high-quality specimens of Ni nanoparticles (Ni-NP) embedded in amorphous SiO_2. Several physical characterizations performed on diluted samples of Ni:SiO_2, with Ni concentrations of ~ 1.5 and 5 wt %, indicated that they have an average radius close to 3 nm, exhibit superparamagnetism (SPM), and are free from an oxide (NiO) layer.

In the modified sol–gel method developed for preparing high-quality Ni:SiO_2 nanocomposites, silicon oxianions and the metal cations (Ni) are immobilized within a polymeric matrix based on polyester. Initially, citric acid was dissolved in ethanol, then tetraethylorthosilicate (TEOS) and nickel nitrate were mixed together. This process assures a good control of both the concentration and the dispersion of the metal through the homogenization of the silica precursor and the metal salt in an ethanolic solution. The polyesterification reaction was promoted by the addition of ethylene glycol to the citrate alcoholic solution. The resulting polymer was pyrolyzed in N_2 atmosphere at different temperatures and times: typically at 500 °C for 2 h. During the pyrolysis, the burn-out of the organic material results in a rich CO/CO_2 atmosphere, which promotes the reduction of the Ni citrate, resulting in nanometric Ni particles [11]. The microstructural characterization was performed on two selected samples S1 (1.5 wt % Ni) and S2 (5 wt % Ni) by means of X-ray diffraction (XRD) and transmission electron microscopy (TEM). The magnetic properties were studied by magnetization measurements $M(T, H)$ in applied magnetic fields $-7\,T \leq H \leq 7\,T$ and at temperatures $2\,K \leq T \leq 300\,K$.

The Ni citrate reduction and the metallic phase formation were analyzed by XRD, as shown in Fig. 1. The diffraction patterns of sample S1, subjected to different pyrolysis temperatures, show the thermal evolution of the most prominent Ni Bragg peaks occurring at $2\theta \sim 44.5°$ (111) and 51.8° (200). The XRD diagrams also revealed no evidence of probable additional phases as NiO. A narrowing of the diffraction peaks with increasing pyrolysis tem-

✉ Fax: +55-11/3091-6984, E-mail: rjardim@if.usp.br

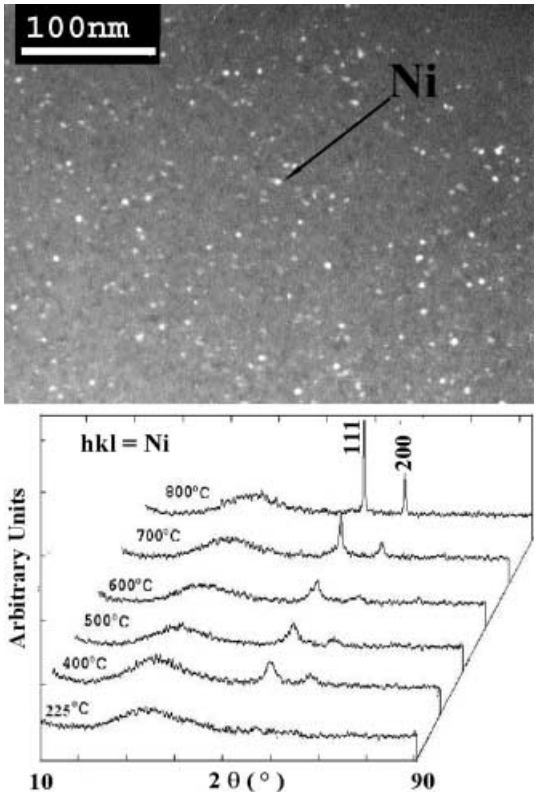

FIGURE 1 Dark-field TEM image of the S1 specimen. The figure also shows the XRD patterns of the specimen as a function of the pyrolysis temperature

perature is also observed and related to the enhanced particle growth. The crystallite sizes of samples pyrolyzed at 500 °C were calculated from the XRD data by using the Scherrer equation, yielding values of crystallite radii $r_{XR} \sim 2.7$ and 2.3 nm for samples S1 and S2, respectively.

The dark-field TEM analysis is also shown in Fig. 1 and revealed two important features of the nanocomposites: (i) homogeneous and randomly dispersed Ni-NP (bright spots in the photograph) throughout the SiO_2 matrix and (ii) a narrow particle SD, with a mean particle size in the range of $r_{mT} \sim 3$ nm, as shown in Fig. 2. The r_{mT} values are slightly higher but consistent with the average crystallite sizes determined by the Scherrer equation, as displayed in Table 1.

The particle SDs shown in Fig. 2 were built from TEM examinations by considering more than 400 particles. The log-normal SDs have distinct characteristics for the studied samples (Table 1). For the sample S1, the median particle size $r_{0T} = 3.9$ nm is close to the mean particle size $r_{mT} = 4.2$ nm due to a small distribution width $\sigma_T = 0.35$ nm. The Ni-richest sample S2 (not shown) revealed a SD with $r_{0T} = 2.3$ nm, $r_{mT} = 3.3$ nm, and a larger distribution width $\sigma_T = 0.84$ (see Table 1).

The magnetic properties of these samples are also of interest. The zero-field cooling (ZFC) branches of the $M(T)$ curves displayed in Fig. 3 exhibit a rounded maximum at T_B, defined as the blocking temperature, which separates the blocking process of small particles ($T < T_B$) from the SPM behavior ($T > T_B$). These $M(T)$ curves also reveal that T_B increases with increasing Ni content, being ~ 20 K and 40 K for samples S1 and S2, respectively. This shift of T_B to higher values is consistent with a larger Ni content of sample S2 and a weak dipolar interaction between particles [12].

Further evidence of the SPM behavior above T_B was inferred from hysteresis loops shown in the inset of Fig. 3. The M/M_S vs. H/T data, for $T > T_B$, resulted in a universal curve, a feature of the SPM response [13]. The magnetic moment distributions were fitted by considering a log-normal weighted Langevin function (log-normal $L(x)$) [13]. From these fittings, the radius distributions of spherical particles were calculated using the saturation magnetization of bulk Ni at 300 K ($M_S = 521$ emu/cm^3). The mean radii r_m were estimated to be 3.8 nm and 4.4 nm for samples S1 and S2, respectively, in excellent agreement with the ones obtained from XRD and TEM analyses. A comparison between the log-normal SDs inferred by either TEM analysis and magnetic-data fitting for the more diluted sample S1 is shown in Fig. 2. The excellent agreement between the two log-normal SDs lends credence to our analysis and may be attributed to both a narrow SD and a negligible interaction between particles [13]. The same analysis, for the

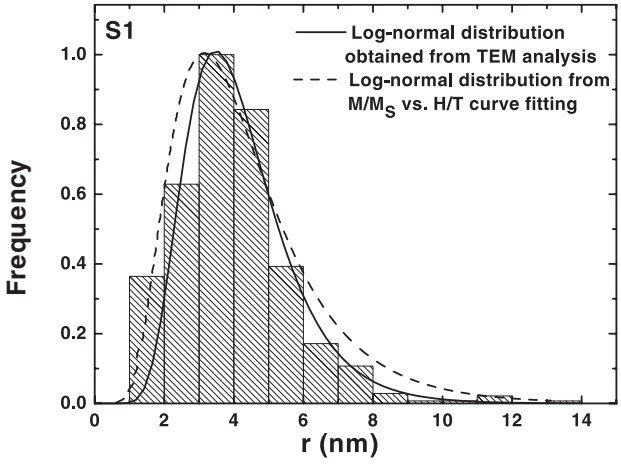

FIGURE 2 Histogram of the size distribution of Ni nanoparticles and log-normal fitting (*solid line*) for the sample S1 determined from TEM analysis. *Dashed line* represents the log-normal size distribution calculated from the log-normal weighted Langevin $L(x)$ fitting for M/M_S vs. H/T curves (see text for details)

Sample	Log-normal $L(x)$					TEM analysis			XRD
	μ_0	r_0	μ_m	r_m	σ	r_{0T}	r_{mT}	σ_T	r_{XR}
S1	4.6	2.8	12	3.8	1.4	3.9	4.2	0.35	2.7
S2	5.1	2.9	17	4.4	1.6	2.3	3.3	0.84	2.3

TABLE 1 Nanoparticle size distribution parameters. Magnetic moment values in emu $\times 10^{17}$ and radii in nm

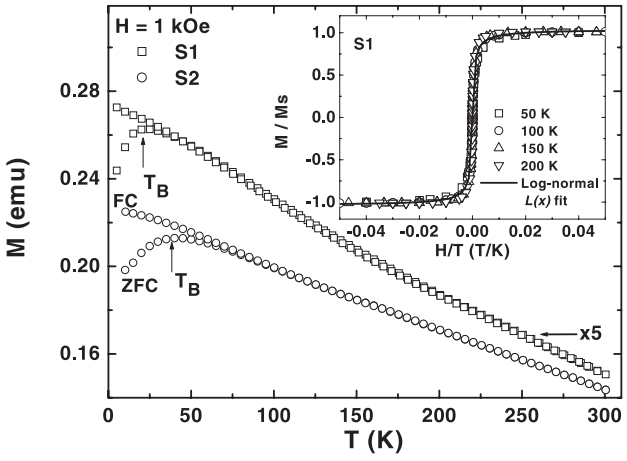

FIGURE 3 Temperature dependence of the magnetization for samples S1 and S2. Curves were taken in ZFC and field-cooling (FC) processes at $H = 1$ kOe. The *inset* shows a universal M/M_S vs. H/T curve, for several temperatures, of the S1 specimen

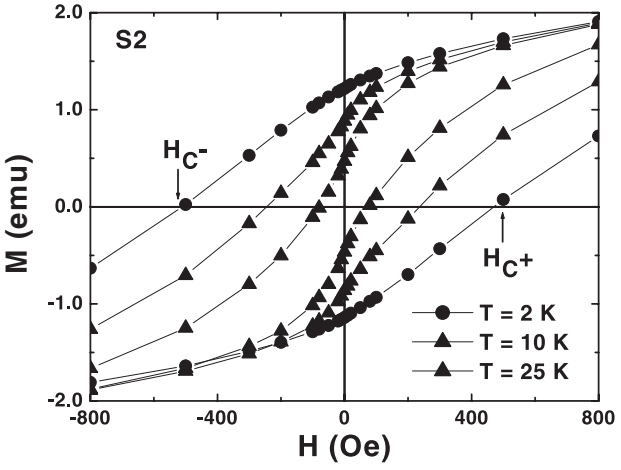

FIGURE 4 Magnetic hysteresis loops measured at 2, 10, and 25 K for the sample S2. The figure also indicates the coercive fields H_{C+} and H_{C-}. The data were collected after ZFC for each measuring temperature

more-concentrated specimen S2 (not shown) resulted in a poorer agreement, with r_0 being slightly higher than r_{0T} but close to r_{mT} (see Table 1). Such a small discrepancy is certainly related to either a magnetic contribution arising from larger particles or weak dipolar interactions [13].

Hysteresis loops taken at several temperatures below T_B are displayed in Fig. 4. The $M(H)$ data exhibit features of SPM particles, such as symmetrical hysteresis loops along the field axis and a decreasing H_C with increasing T. It is important to notice that Ni-NP with NiO coatings are observed to exhibit an asymmetry along the field axis (exchange bias) due to the exchange interactions between FM-Ni and AFM-NiO [14]. An estimate of the loop symmetry is done by defining $\Delta H_C = (H_{C+} + H_{C-})/2$, where H_{C+} and H_{C-} are the coercive fields with decreasing and increasing H, respectively. Previous work on partially oxidized Ni-NP reported $\Delta H_C \sim 700$ Oe [15], a value much larger than $\Delta H_C \sim 1$ Oe found in our samples. The $M(H)$ data also indicate negligible contributions arising from isolated NiO-NP, which would produce an appreciable shift in the $M(H)$ data [14]. Thus, our results for $M(H)$ strongly suggest that the sol–gel technique used here also prevents the formation of an oxide layer in Ni-NP dispersed in SiO_2.

In summary, a modified sol–gel method to prepare high-quality Ni:SiO_2 nanocomposites has been developed. The obtained Ni-NP have a mean radius of ~ 3 nm, narrow particle SDs, and exhibit SPM behavior above T_B ($T_B < 40$ K). The Ni-NP size distributions, determined from magnetic measurements, were in excellent agreement with those obtained from TEM analysis. Due to the absence of a shift along the field axis in the $M(H)$ curves below T_B and the XRD data, we have also inferred that these Ni-NP are free from an oxide layer.

ACKNOWLEDGEMENTS We are grateful to A.L. Brandl, J. Cesar, and M. Knobel for the program codes for distribution calculations. This work was supported in part by the Brazilian agency FAPESP under Grant Nos. 99/10798-0, 01/02598-3, 98/14324-0, and 01/04231-0. Three of us (R.F.J., G.F.G., and E.R.L.) are fellows of the Conselho Nacional de Desenvolvimento Científico e Tecnológico (CNPq).

REFERENCES

1 C.B. Murray, S. Sun, H. Doyle, T. Betley: MRS Bull. **26**, 985 (2001)
2 D.L. Leslie-Pelecky, R.D. Rieke: Chem. Mater. **8**, 1770 (1996)
3 M.E. McHenry, S.A. Majetich, J.O. Artman, M. DeGraef, S.W. Staley: Phys. Rev. B **49**, 11 358 (1994)
4 S. Linderoth, L. Balcells, A. Labarta, J. Tejada, P.V. Hendriksen, S.A. Sethi: J. Magn. Magn. Mater. **124**, 269 (1993)
5 T. Hayashi, T. Ohno, S. Yatsuya, R. Ueda: Jpn. J. Appl. Phys. **16**, 705 (1977)
6 A. Gavrin, C.L. Chien: J. Appl. Phys. **73**, 6949 (1993)
7 S. Sun, C.B. Murray, D. Weller, L. Folks, A. Moser: Science **287**, 1989 (2000)
8 S. Sun, C.B. Murray: J. Appl. Phys. **85**, 4325 (1999)
9 E. Cattaruzza, F. Gonella, G. Mattei, P. Mazzoldi, D. Gatteschi, C. Sangregorio, M. Falconieri, G. Salvetti, G. Battaglin: Appl. Phys. Lett. **73**, 1176 (1998)
10 C.A. Morris, M.L. Anderson, R.M. Stroud, C.I. Merzbacher, D.R. Rolison: Science **284**, 622 (1999)
11 E.R. Leite, N.L.V. Carreño, E. Longo, A. Valentini, L.F.D. Probst: J. Nanosci. Nanotechnol. **2**, 89 (2002)
12 J.I. Gittleman, B. Abeles, S. Bozowski: Phys. Rev. B **9**, 3891 (1974)
13 F.C. Fonseca, G.F. Goya, R.F. Jardim, R. Muccillo, N.L.V. Carreño, E. Longo, E.R. Leite: Phys. Rev. B **66**, 104406 (2002)
14 R.H. Kodama, S.A. Makhlouf, A.E. Berkowitz: Phys. Rev. Lett. **79**, 1393 (1997)
15 Y.D. Yao, Y.Y. Chen, M.F. Tai, D.H. Wang, H.M. Lin: Mater. Sci. Eng. A **217**, 837 (1996)